

Article

Controlling the Polymer Ink's Rheological Properties to Form Single and Stable Droplet

Zhonghui Du ¹, Lu Zhang ², Yushuang Du ³, Xiaoqing Wei ¹, Xiang Du ¹, Xinyan Lin ¹, Jiajun Liu ¹, Yani Huang ¹, Yan Xue ^{1,*}, Ning Zhao ^{1,*} and Hongbo Liu ^{1,*}

¹ School of Materials & Environmental Engineering, Shenzhen Polytechnic University, Shenzhen 518055, China; duzhonghui@szpu.edu.cn (Z.D.); aprilwei@szpu.edu.cn (X.W.); df2003110@szpu.edu.cn (X.D.); lin2618@szpu.edu.cn (X.L.); lzp790310@szpu.edu.cn (J.L.); huangguanlan@szpu.edu.cn (Y.H.);

² Department of Power Mechanical Engineering, Beijing Jiaotong University, Beijing 100044, China; 22110424@bjtu.edu.cn

³ School of Chemistry Engineering, East China University of Science and Technology, Shanghai 200237, China; dyushuang@163.com

* Correspondence: xueyan@szpu.edu.cn (Y.X.); zhaoning@szpu.edu.cn (N.Z.); liuhongbo@szpu.edu.cn (H.L.)

Abstract: The formation of single and stable ink droplets is crucial for producing high-quality functional films in drop-on-demand (DOD) inkjet printing. The stability and singularity of droplet formation are significantly influenced by filament breakup behavior, governed by the rheological parameters of the ink formula. This study explores the droplet formation behavior of Poly3-hexylthiophene (P3HT) ink across various Weber numbers (We) and assesses the impact of the Z value on the formation of single ink droplets. Observations reveal that as the We number increases, droplet morphology transitions from single to double, and eventually to sputtered droplets. Results demonstrate that stable, single droplets form when the We number ≤ 13 and $12 < Z < 34$, with a pulse duration of approximately 340 μ s. When the We number exceeds 13, the molecular chains of P3HT stretch due to high hydrodynamic forces, resulting in the formation of unwanted satellite droplets.

Keywords: inkjet printing; We number; single droplet; satellite droplets



Citation: Du, Z.; Zhang, L.; Du, Y.; Wei, X.; Du, X.; Lin, X.; Liu, J.; Huang, Y.; Xue, Y.; Zhao, N.; et al. Controlling the Polymer Ink's Rheological Properties to Form Single and Stable Droplet. *Coatings* **2024**, *14*, 600. <https://doi.org/10.3390/coatings14050600>

Academic Editors: Tsvetanka Babeva, Gergana Alexieva and Rositsa Gergova

Received: 16 April 2024

Revised: 6 May 2024

Accepted: 7 May 2024

Published: 10 May 2024



Copyright: © 2024 by the authors. Licensee MDPI, Basel, Switzerland. This article is an open access article distributed under the terms and conditions of the Creative Commons Attribution (CC BY) license (<https://creativecommons.org/licenses/by/4.0/>).

1. Introduction

Because of its unique advantages, inkjet printing technology has been widely used in fine pattern processing, such as biochemical for cell guidance [1–3], organic light-emitting diodes [4–6], solar cells [7–9], sensors [10–13] and so on. In drop-on-demand (DOD) inkjet printer, with the mechanical deformation of the piezoelectric transducer in the ink chamber, the ink droplet is squeezed out when an electric voltage signal is applied to the piezoelectric transducer. Forming single and stable ink droplet is the key to printing high-quality functional films in drop-on-demand (DOD) inkjet printing [14–16].

In the early research, inks with no solute were often used in DOD inkjet printing [17–22]. Morris, Jeffrey F. et al. used the glycerin–water and glycerin–water–isopropanol mixtures as the inks and the main stages of DOD drop formation were analyzed [23]. The main stages of DOD drop formation include the ejection and stretching of liquid, the pinch-off of liquid thread from the nozzle exit, the contraction of liquid thread, the breakup of liquid thread into primary drop and satellites, and the recombination of primary drop and satellites. Daehwan Jang et al. have investigated the inter-relationship between inkjet printability and physical fluid properties by monitoring droplet formation dynamics using a mixture of ethyl alcohol and ethylene glycol [24]. Berend-Jan de Gans et al. have investigated the influence of architecture on the inkjet printability of polymer solutions by comparing linear and 6-arm star PMMA inks [25].

For certain inks, their physical characteristic parameters intricately affect the droplet formation process [26–28]. To simplify the influence process, dimensionless parameters

were proposed to elucidate the dynamics of droplet formation [29–34]. One such parameter is the Weber number (We), representing the ratio of inertial and capillary forces, expressed as follows:

$$We = \frac{v^2 \alpha \rho}{\gamma} \quad (1)$$

The Reynolds number (Re) is utilized to characterize fluid flow, representing the ratio of inertial to viscous forces, and is expressed as follows:

$$Re = \frac{v \alpha \rho}{\eta} \quad (2)$$

Z is defined as the ratio of the Reynolds number to the square root of the Weber number.

$$Z = \frac{Re}{We^{1/2}} = \frac{(\gamma \rho \alpha)^{1/2}}{\eta} \quad (3)$$

In the above formulas, v is the droplet velocity, α is the characteristic length (e.g., the diameter of the jetting nozzle), ρ is the fluid density, η is the fluid viscosity, and γ is the surface tension. Proper parameters are crucial for achieving stable injection. Fromm originally proposed that inkjet printing is possible if $Z > 4$ [35]. These limits have been experimentally studied, and a slightly wider range has been proposed with $1 < Z < 14$ [36]. To generate a small radius droplet, the surface tension and associated Laplace pressure must be overcome before a drop can be ejected from a printer. Duineveld proposed that this can be described by a minimum value of the Weber number, $We > 4$, below which there is insufficient fluid flow to overcome surface tension [37]. When $We < 4$, the droplet cannot be injected from the nozzle.

Ink properties substantially influence the quality of droplet formation in inkjet printing, with optimal performance parameters varying across different ink formulations [38–40]. This study investigates how the physical properties of inks influence droplet formation, focusing specifically on conditions enabling a stable and single droplet ejection of Poly3-hexylthiophene (P3HT) ink. We have comprehensively examined the roles of the dimensionless Weber number (We) and the Z value in the dynamics of droplet formation. This analysis not only enhances our understanding of P3HT ink behavior but also yields valuable insights applicable to optimizing printing processes for other functional materials. By exploring the interplay between these parameters, our research aims to delineate the ‘printable window’ for P3HT inks, defined as the specific range of conditions under which the ink exhibits optimal jetting performance without forming satellite droplets or other anomalies. Understanding these conditions is expected to facilitate precise material deposition in applications ranging from electronics to biomedical devices, where the exact placement and structure of materials are critical [41,42]. The findings of this study could serve as a foundational reference for further experimental and theoretical research on the fluid dynamics of inkjet printing.

2. Materials and Methods

The P3HT ink solution was meticulously prepared by solving Poly3-hexylthiophene (P3HT) with chlorobenzene (CB) solvent at ambient temperature. The P3HT powder was synthesized to have a molecular weight (MW) of 102 kDa and a polydispersity index (PDI) of 2.19. The CB solvent was procured from Sigma-Aldrich Co., Ltd. (St. Louis, Missouri, USA) without any additional purification of the solvent. The solution was concentrated at 5 mg/mL using the specified 102 kDa molecular weight P3HT material. To ensure the complete dissolution of the P3HT, the mixture was gently heated for 10 min and then allowed to rest at room temperature for 24 h before use. This procedure ensures that the ink has the appropriate viscosity and chemical consistency for optimal printing performance.

The inkjet printing experiments were conducted using the AD-P-8000 Printing System (Cambridge, UK) with a high-resolution built-in CCD shown in Figure 1, provided by

Microdrop Technologies GmbH. Its nozzle diameter is 50 μm . Its viscosity and surface tension range are 0.4–100 mPa·s and 28–72 mN/m. And its max printing frequency is 2000 Hz. To prevent the clogging of the printing head—an issue that can impede consistent droplet formation—the ink solutions were filtered through a 0.2 μm filter prior to use. This filtering step ensures a clean, smooth flow of ink through the printing system.

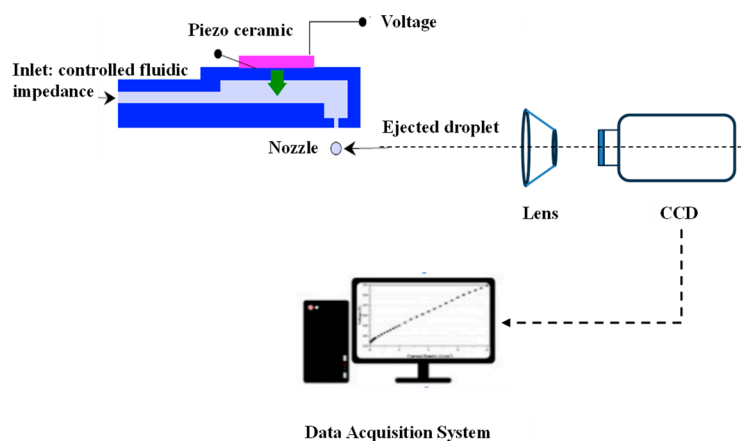


Figure 1. Schematic diagram of the experimental setup.

During the experiment, the formation of ink droplets under various driving voltages was meticulously captured using a high-speed CCD camera. This advanced imaging setup allowed for the detailed observation of the droplet dynamics with an interframe time of just 2 microseconds between each image. Such high temporal resolution is crucial for accurately analyzing the rapid processes involved in droplet formation and detachment from the nozzle.

The viscosity of the inks was meticulously characterized using the LVDV-III+ Programmable Control Rheometer from Brookfield Ltd. (Toronto, Canada) This measurement was conducted at room temperature, ensuring the ink's rheological properties were assessed under standard conditions to maintain consistency and reliability in data.

Additionally, the surface tension of the P3HT inks was accurately determined using the pendant drop method with the assistance of the DSA10 liquid drop shape analyzer from KRUSS GmbH, Hamburg, Germany. This method involves meticulously forming a single ink droplet at the tip of a needle or nozzle, which is then analyzed to determine its shape. The shape of the pendant droplet serves as a crucial indicator of surface tension. To ensure the highest accuracy of these measurements, a complete droplet of ink was extruded during the testing process to minimize potential errors caused by partial droplet formation or interference from environmental factors. The physical parameters of the Poly3-hexylthiophene (P3HT) ink are shown in Table 1.

Table 1. Physical parameters of the Poly3-hexylthiophene (P3HT) ink.

Parameters	Value
Density, ρ	1068.40 Kg/m ³
Surface tension, γ	31.0 mN/m
Viscosity, η	1.20 mPa·s
Conductivity, G	450 S/m
Z value	33.91

As previously stated, in drop-on-demand (DOD) inkjet printing, the production of uniform and stable ink droplets is crucial for fabricating high-quality functional films. The morphology of these droplets is chiefly influenced by ink viscosity, surface tension, and ejection velocity, with the Weber number (We), a dimensionless quantity representing the

relative importance of inertial forces to surface tension, commonly employed to comprehend the droplet shape and stability. This study, by regulating the ink ejection velocity, examines the droplet ejection characteristics of P3HT ink under various Weber number conditions as depicted in Table 2, thereby enhancing the understanding and controlling of its application in DOD inkjet printing processes.

Table 2. The value of We for the Poly3-hexylthiophene (P3HT) at different dropping velocities.

Velocity (m/s)	Re	We
1.1	50.8	2.2
1.8	81.1	5.7
2.3	103.1	9.3
2.6	115.8	11.7

The concentration of the ink directly affects the Z value, and the change in the Z value will influence the inkjet printing dynamic process of the ink. Inks with different Z values were also investigated in Table 3.

Table 3. Z value of different concentrations of Poly3-hexylthiophene (P3HT).

Concentration (mg/mL)	Z
5	33.91
10	24.31
15	18.30
20	12.75

3. Results and Discussion

Firstly, we investigated the influence of We number on the ink droplet formation using the P3HT ink solution. The ink solution was prepared with a concentration of 5 mg/mL, dissolving 102 kDa molecular weight P3HT material. Our analysis was visually documented through a series of high-resolution jetting images, collectively referred to as Figure 2. These images captured the dynamic evolution of droplet formation at varying Weber numbers: 2.2, 5.7, 9.3, and 11.7. The imaging interval was maintained at 20 μ s, covering a range from 80 to 500 μ s to observe the droplet formation and fusion process in real-time. In Figure 2a, the initial formation of a liquid column is evident at 80 μ s. A mere 20 μ s later, a ligament extends from the nozzle, indicating the beginning of droplet separation. By 140 μ s, a secondary, smaller droplet is visible trailing the primary droplet. This secondary droplet gains kinetic energy, progressively closing the distance to the primary droplet. By 300 μ s, the two droplets merge into a single, larger droplet due to the kinetic energy surplus. This phenomenon of droplet fusion, driven by the Weber number, recurs in subsequent images (Figure 2b–d), illustrating a consistent pattern across different We values.

To provide a quantitative perspective on these observations, we meticulously measured the distances between the primary and secondary droplets during the jetting process. These measurements are graphically represented in Figure 3, which plots the distance of each droplet from the nozzle against time. The trajectory of the primary droplet is depicted with a black line, while the trajectory leading to the formation of the secondary droplet is marked in red. Our analysis highlights a notable trend for the sample with $We = 2.2$, where the gap between the primary and secondary droplets decreases steadily over time until the primary and the second droplets merge. The same phenomenon occurs in Figure 3b–d. This trend underscores the substantial influence of the Weber number on the dynamics of droplet formation and fusion.

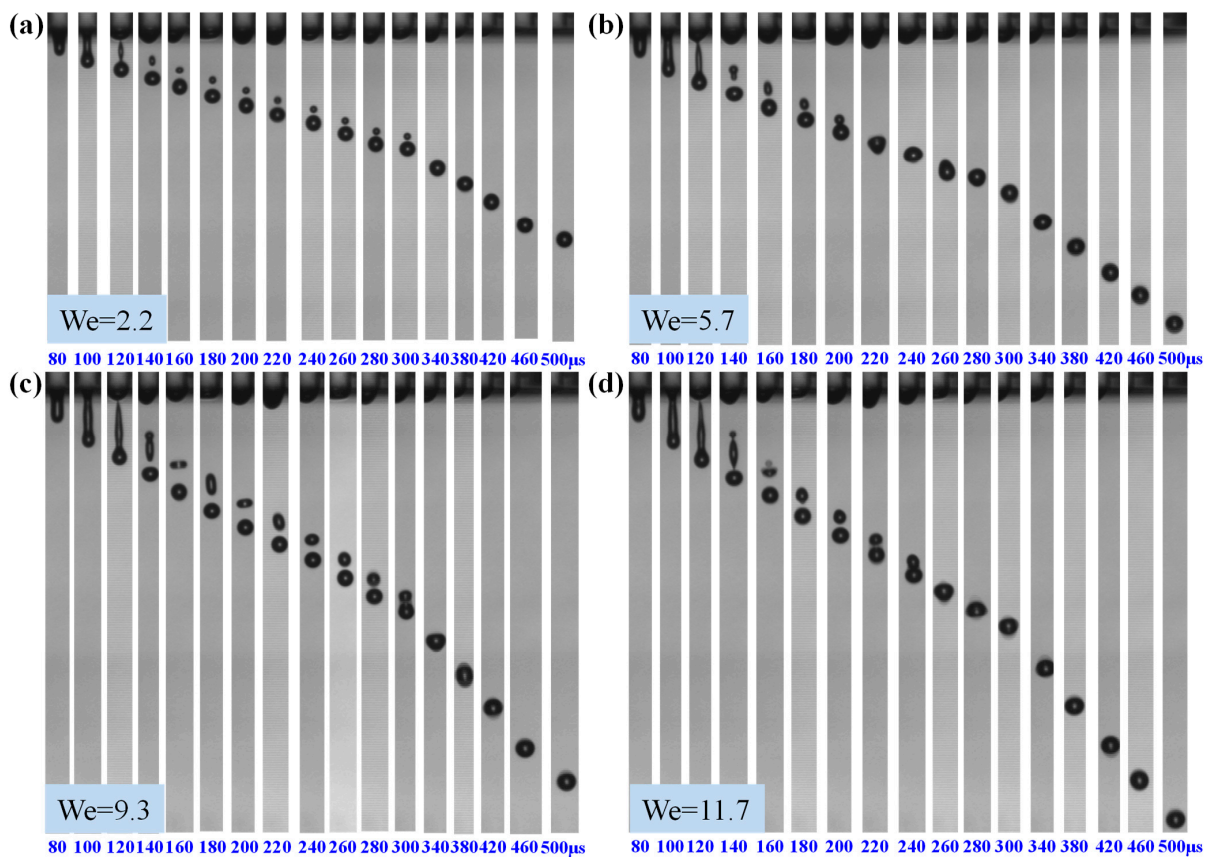


Figure 2. Droplet formation behavior at different We numbers, (a) $We = 2.2$, (b) $We = 5.7$, (c) $We = 9.3$, and (d) $We = 11.7$.

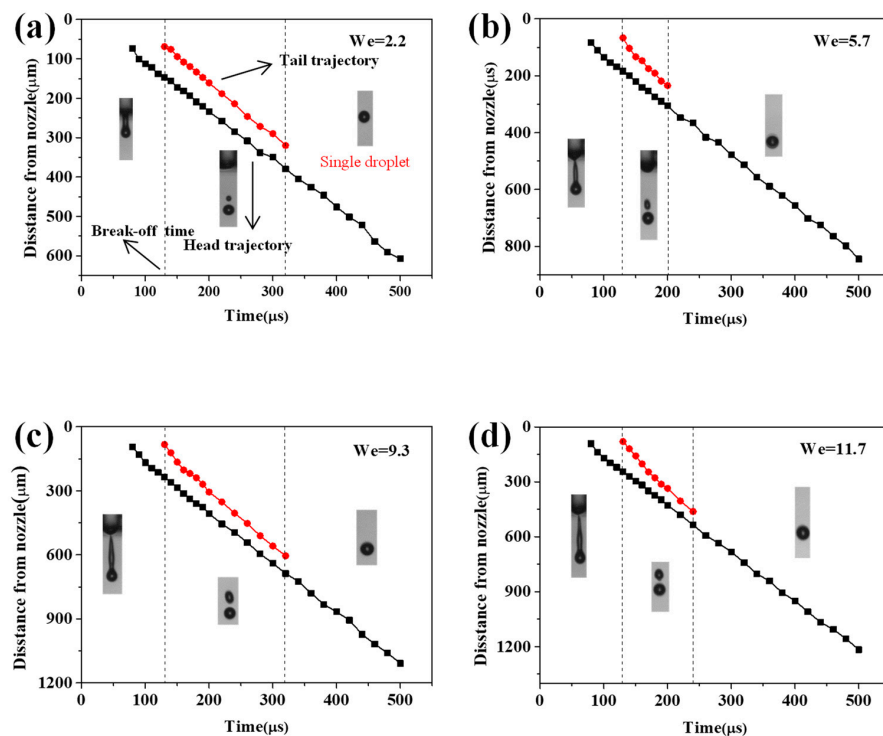


Figure 3. Trajectories (the black lines: head trajectory, the red lines: tail trajectory) of ejected droplets versus inkjetting time for inks with different Weber numbers, (a) $We = 2.2$, (b) $We = 5.7$, (c) $We = 9.3$, and (d) $We = 11.7$.

Figure 4 details the formation dynamics of P3HT ink droplets at We numbers of 13.4 and 36.5. Initially, a primary droplet forms, connected to the nozzle by a ligament, observed at 80 μs and 100 μs . By 160 μs , a smaller secondary droplet emerges, trailing behind the primary droplet. Unlike the scenarios depicted in Figure 1, these primary and secondary droplets do not merge into a single droplet, even after 500 μs . This persistent separation leads to the formation of an additional, third droplet at durations of 180 μs and 200 μs in Figure 4b.

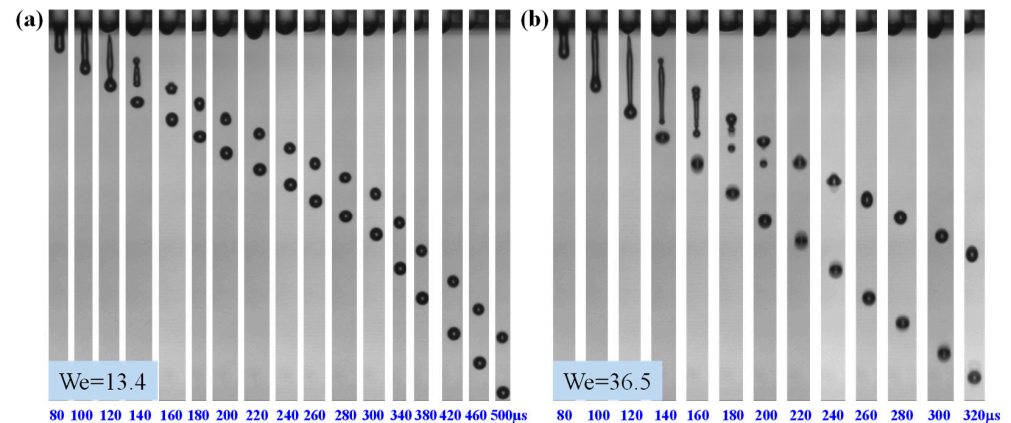


Figure 4. Droplet formation behavior at higher Weber numbers, specifically (a) $We = 13.4$ and (b) $We = 36.5$.

Figure 5 further explores the distances these droplets travel from the nozzle. The behavior of the droplets is classified into two distinct regions: the filament and the double droplet regions. In the filament region, the droplet forms a lengthy filament extending from the nozzle, significantly longer than those depicted in Figure 2. In the double droplet region, the separation between the primary droplet's leading edge and the secondary droplet's trailing edge significantly widens as time progresses. This increasing gap primarily prevents the droplets from merging, ultimately resulting in the formation of two distinct droplets. This behavior underscores the complex interplay between the kinetic energy and fluid dynamics at higher Weber numbers. The failure to merge at higher We values illustrates the limitations of the cohesive forces within the ink, exacerbated by the increased kinetic energy that propels the droplets apart rather than allowing them to coalesce. These observations are crucial for understanding the limitations and challenges in tuning ink formulations and printing parameters to achieve the desired outcomes, particularly in high-resolution printing applications where droplet precision is paramount.

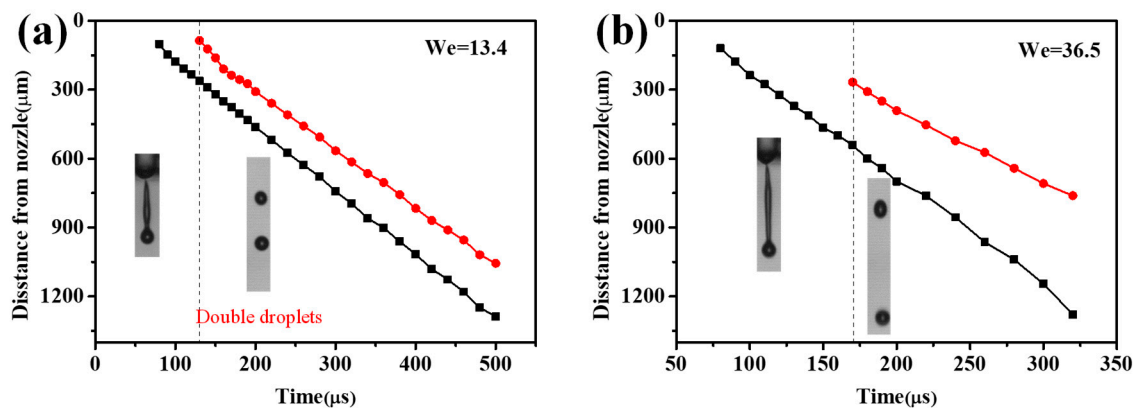


Figure 5. Trajectories (the black lines: head trajectory, the red lines: tail trajectory) of ejected droplets versus inkjetting time for inks with Weber numbers of (a) 13.4 and (b) 36.5.

To investigate the influence of kinetic energy on droplet volume, we analyzed the correlation between the droplet radius and the We number. As illustrated in Figure 6, a clear trend emerges: the droplet radius increases gradually with the We number. For example, at a We number of 3, the droplet radius measures 44 μm , which increases to 54 μm when the We number reaches 11.7, corresponding to a 50% increase in droplet volume. This progression suggests that higher Weber numbers correspond to increased kinetic energy affecting the droplet, thereby leading to an expansion in droplet volume.

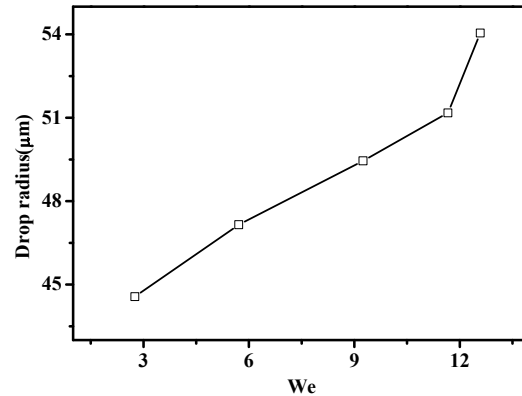


Figure 6. The relationship between the droplet radius and the We number.

Figure 7 presents a comprehensive summary of the droplet behavior under varying Z values and We numbers for P3HT ink, illustrating the impact of these parameters on inkjet printing dynamics. The observed droplet behaviors can be classified into three distinct scenarios: the formation of a single droplet, the formation of double droplets, and splashing events. Notably, when the Weber number exceeds 13, depicted by blue dots in the figure, a splashing phenomenon emerges. This phenomenon is characterized by numerous small, scattered droplets, indicative of excessive kinetic energy that disrupts droplet cohesion and results in erratic deposition patterns.

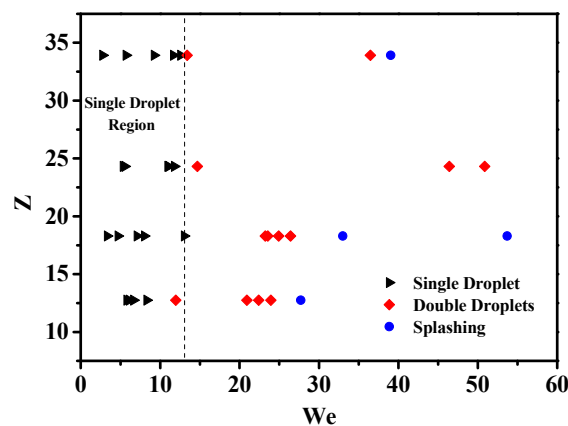


Figure 7. The printable region as a function of the We number relationship with respect to Z .

Conversely, when the Weber number is below 13 and $12 < Z < 34$, the ink demonstrates the formation of single, stable droplets. This situation represents the optimal conditions for controlled droplet deposition, crucial for achieving precision in applications such as electronic circuitry fabrication or the layering of sensitive biochemical substrates. The stability of these droplets ensures that the deposited materials adhere to precise locations and configurations, which are critical for the functionality and reliability of the final products.

This differentiation in droplet behaviors underscores the critical importance of fine-tuning the printing parameters, especially the Weber number, to align with the specific

requirements of the printing task. By selecting the appropriate Weber number, manufacturers can manipulate droplet formation to mitigate unwanted splashing and ensure high-quality printing with minimal material waste.

4. Conclusions

In this study, we systematically investigated the influence of the Weber number (We) on droplet formation in inkjet printing processes. As the We number increases, droplet morphology transitions from single to double, and eventually to sputtered droplets. As for single droplet formation, the droplet radius increases gradually with the We number. Our comprehensive analysis across various driving voltages revealed that a Weber number (We) below 13 and $12 < Z < 34$ provides an optimal range for achieving the consistent formation of single droplets. Specifically, a pulse duration of 38.5 μs , employing a single waveform, is adequate for forming the stable droplets of P3HT ink without the presence of satellite droplets or other instabilities.

These findings not only confirm the crucial role of the Weber number in determining the printing capabilities of P3HT inks but also establish clear guidelines for its application in precision inkjet printing. They offer a framework for predicting and controlling the fidelity of droplet formation, which is especially valuable for the development of printing protocols for advanced materials, where the fidelity of droplet formation directly impacts the quality and functionality of the final product.

Author Contributions: Z.D., L.Z., Y.D., X.W., X.D., X.L., J.L. and Y.H. contributed to the experiment design, data analysis, and writing. The material preparation and data collection were performed by Y.X., N.Z. and H.L. All authors have read and agreed to the published version of the manuscript.

Funding: This work was supported by the Shenzhen Polytechnic Research Fund (6023310025K) and Post-doctoral Later-stage Foundation Project of Shenzhen Polytechnic (6023271017K), the funding from the Basic and Applied Basic Research Funding of Guangdong (No.2020A1515110551), Provincial Education Department of Guangdong (No.2021KTSCX277), Shenzhen Science and Technology Program (No.RCBS20210609103648040), and Provincial High Vocational Education Teaching Reform Research and Practice Project (GDJG2021422). Key funded projects of special funds for scientific and technological innovation strategy of Guangdong Province (pdjh2022a0973, pdjh2022001, pdjh2023a0967), Shenzhen Science and Technology Program under grant (KJZD20230923114412026), Post-doctoral Later-stage Foundation Project of Shenzhen Polytechnic under grant (6021271013K), and the Founding of Shenzhen polytechnic (No. 6021310007K, 6022312061K, 6022310034K, 6021271011K, 6021230059K, 6021210078K, LHRC20220402, 1019-8122310001C0, 6022310030K) provided funding for this work.

Institutional Review Board Statement: Not applicable.

Informed Consent Statement: Not applicable.

Data Availability Statement: All data generated or analyzed during this study are included in this article.

Conflicts of Interest: The authors declare that they have no known competing financial interests or personal relationships that could have appeared to influence the work reported in this paper.

References

1. Saunders, R.E.; Derby, B. Inkjet printing biomaterials for tissue engineering: Bioprinting. *Int. Mater. Rev.* **2014**, *59*, 430–448. [[CrossRef](#)]
2. Zhang, G.; Qu, Z.; Tao, W.-Q.; Wang, X.; Wu, L.; Wu, S.; Xie, X.; Tongsh, C.; Huo, W.; Bao, Z.; et al. Porous Flow Field for Next-Generation Proton Exchange Membrane Fuel Cells: Materials, Characterization, Design, and Challenges. *Chem. Rev.* **2022**, *123*, 989–1039. [[CrossRef](#)] [[PubMed](#)]
3. Xu, C.; Zhang, M.; Huang, Y.; Ogale, A.; Fu, J.; Markwald, R.R. Study of Droplet Formation Process during Drop-on-Demand Inkjetting of Living Cell-Laden Bioink. *Langmuir* **2014**, *30*, 9130–9138. [[CrossRef](#)] [[PubMed](#)]
4. Wang, J.J.; Li, D.Y.; Mu, L.; Li, M.Z.; Luo, Y.; Zhang, B.B.; Mai, C.H.; Guo, B.A.; Lan, L.F.; Wang, J.; et al. Inkjet-Printed Full-Color Matrix Quasi-Two-Dimensional Perovskite Light-Emitting Diodes. *ACS Appl. Mater. Interfaces* **2021**, *13*, 41773–41781. [[CrossRef](#)] [[PubMed](#)]

5. Xue, Y.; Wang, L.; Zhang, Y.; Liang, G.; Chu, J.; Han, B.; Cao, W.; Liao, C.; Zhang, S. 31-Inch 4K Flexible Display Employing Gate Driver With Metal Oxide Thin-Film Transistors. *IEEE Electron Device Lett.* **2021**, *42*, 188–191. [[CrossRef](#)]
6. Cai, X.; Su, S.-J. Marching Toward Highly Efficient, Pure-Blue, and Stable Thermally Activated Delayed Fluorescent Organic Light-Emitting Diodes. *Adv. Funct. Mater.* **2018**, *28*, 1802558. [[CrossRef](#)]
7. Aernouts, T.; Aleksandrov, T.; Giroto, C.; Genoe, J.; Poortmans, J. Polymer based organic solar cells using ink-jet printed active layers. *Appl. Phys. Lett.* **2008**, *92*, 03306. [[CrossRef](#)]
8. Hoth, C.N.; Schilinsky, P.; Choulis, S.A.; Brabec, C.J. Printing Highly Efficient Organic Solar Cells. *Nano Lett.* **2008**, *8*, 2806–2813. [[CrossRef](#)]
9. Krebs, F.C. Fabrication and processing of polymer solar cells: A review of printing and coating techniques. *Sol. Energy Mater. Sol. Cells* **2009**, *93*, 394–412. [[CrossRef](#)]
10. Tu, N.; Lo, J.C.C.; Lee, S.W.R. Development of Uniform Polydimethylsiloxane Arrays through Inkjet Printing. *Polymers* **2023**, *15*, 462. [[CrossRef](#)]
11. Gupta, S.; Thombare, M.R.; Patil, N.D. Pinning and Depinning Dynamics of an Evaporating Sessile Droplet Containing Mono- and Bidispersed Colloidal Particles on a Nonheated/Heated Hydrophobic Substrate. *Langmuir* **2023**, *39*, 3102–3117. [[CrossRef](#)] [[PubMed](#)]
12. Bai, J.Y.; Hu, H.L.; Yu, Y.S.; Zhu, Y.B.; Xu, Z.W.; Zheng, W.C.; Zhao, H.B.; Lin, L.H.; Guo, T.L.; Li, F.S. Achieving high performance InP quantum dot light-emitting devices by using inkjet printing. *Org. Electron.* **2023**, *113*, 106705. [[CrossRef](#)]
13. Huang, Q.; Al-Milaji, K.N.; Zhao, H. Inkjet Printing of Silver Nanowires for Stretchable Heaters. *ACS Appl. Nano Mater.* **2018**, *1*, 4528–4536. [[CrossRef](#)]
14. Driessen, T.; Jeurissen, R. Drop Formation in Inkjet Printing. In *Fundamentals of Inkjet Printing*; Wiley-VCH Verlag GmbH & Co. KGaA: Weinheim, Germany, 2016; pp. 93–116.
15. Notz, P.K.; Basaran, O.A. Dynamics and breakup of a contracting liquid filament. *J. Fluid Mech.* **2004**, *512*, 223–256. [[CrossRef](#)]
16. Schulkes, R. The contraction of liquid filaments. *J. Fluid Mech.* **1996**, *309*, 277–300. [[CrossRef](#)]
17. Bernasconi, R.; Brovelli, S.; Viviani, P.; Soldo, M.; Giusti, D.; Magagnin, L. Piezoelectric Drop-On-Demand Inkjet Printing of High-Viscosity Inks. *Adv. Eng. Mater.* **2022**, *24*, 2100733. [[CrossRef](#)]
18. Satpathi, N.S.; Malik, L.; Ramasamy, A.S.; Sen, A.K. Drop Impact on a Superhydrophilic Spot Surrounded by a Superhydrophobic Surface. *Langmuir* **2021**, *37*, 14195–14204. [[CrossRef](#)] [[PubMed](#)]
19. Jung, S.J.; Hoath, S.D.; Hutchings, I.M. The role of viscoelasticity in drop impact and spreading for inkjet printing of polymer solution on a wettable surface. *Microfluid. Nanofluidics* **2013**, *14*, 163–169. [[CrossRef](#)]
20. Hoath, S.D.; Jung, S.; Hutchings, I.M. A simple criterion for filament break-up in drop-on-demand inkjet printing. *Phys. Fluids* **2013**, *25*, 5. [[CrossRef](#)]
21. Hoath, S.D.; Hutchings, I.M.; Harlen, O.G.; McLlroy, C.; Morrison, N.F. *Regimes of Polymer Behaviour in Drop-on-Demand Ink-Jetting*; Society for Imaging Science & Technology: Springfield, VA, USA, 2012; pp. 408–411.
22. Hoath, S.; Martin, G.; Castrejon-Pita, R.; Hutchings, I. *Satellite Formation in Drop-on-Demand Printing of Polymer Solutions*; Society for Imaging Science & Technology: Springfield, VA, USA, 2007; pp. 331–335.
23. Dong, H.; Carr, W.W.; Morris, J.F. An experimental study of drop-on-demand drop formation. *Phys. Fluids* **2006**, *18*, 072102. [[CrossRef](#)]
24. Jang, D.; Kim, D.; Moon, J. Influence of Fluid Physical Properties on Ink-Jet Printability. *Langmuir* **2009**, *25*, 2629–2635. [[CrossRef](#)]
25. de Gans, B.J.; Xue, L.J.; Agarwal, U.S.; Schubert, U.S. Ink-jet printing of linear and star polymers. *Macromol. Rapid Commun.* **2005**, *26*, 310–314. [[CrossRef](#)]
26. Suryo, R.; Doshi, P.; Basaran, O.A. Nonlinear dynamics and breakup of compound jets. *Phys. Fluids* **2006**, *18*, 082107. [[CrossRef](#)]
27. Aytouna, M.; Paredes, J.; Shahidzadeh-Bonn, N.; Moulinet, S.; Wagner, C.; Amarouchene, Y.; Eggers, J.; Bonn, D. Drop Formation in Non-Newtonian Fluids. *Phys. Rev. Lett.* **2013**, *110*, 5. [[CrossRef](#)]
28. Du, Z.; Zhou, H.; Cao, W.; Yu, X.; Han, Y. The effects of coil–stretch transition behavior of polyfluorene inks on single droplet formation during inkjet printing. *Chin. Chem. Lett.* **2020**, *31*, 3216–3220. [[CrossRef](#)]
29. Kang, D.J.; Gonzalez-Garcia, L.; Kraus, T. Soft electronics by inkjet printing metal inks on porous substrates. *Flex. Print. Electron.* **2022**, *7*, 033001. [[CrossRef](#)]
30. Yan, K.; Li, J.A.; Pan, L.J.; Shi, Y. Inkjet printing for flexible and wearable electronics. *APL Mater.* **2020**, *8*, 120705. [[CrossRef](#)]
31. Rivadeneyra, A.; Lopez-Villanueva, J.A. Recent Advances in Printed Capacitive Sensors. *Micromachines* **2020**, *11*, 367. [[CrossRef](#)] [[PubMed](#)]
32. Smith, P.J.; Stringer, J. Applications in Inkjet Printing. In *Fundamentals of Inkjet Printing*; Wiley-VCH Verlag GmbH & Co. KGaA: Weinheim, Germany, 2016; pp. 397–418.
33. Shi, Y.; Liu, J.; Yang, Y. Device performance and polymer morphology in polymer light emitting diodes: The control of thin film morphology and device quantum efficiency. *J. Appl. Phys.* **2000**, *87*, 4254–4263. [[CrossRef](#)]
34. Nguyen, T.Q.; Doan, V.; Schwartz, B.J. Conjugated polymer aggregates in solution: Control of interchain interactions. *J. Chem. Phys.* **1999**, *110*, 4068–4078. [[CrossRef](#)]
35. Fromm, J.E. Numerical-Calculation of the Fluid-Dynamics of Drop-On-Demand Jets. *IBM J. Res. Dev.* **1984**, *28*, 322–333. [[CrossRef](#)]
36. Derby, B.; Reis, N. Inkjet printing of highly loaded particulate suspensions. *MRS Bull.* **2003**, *28*, 815–818. [[CrossRef](#)]
37. Derby, B. Inkjet printing ceramics: From drops to solid. *J. Eur. Ceram. Soc.* **2011**, *31*, 2543–2550. [[CrossRef](#)]

38. Du, Z.; Zhou, H.; Yu, X.; Han, Y. Controlling the polarity and viscosity of small molecule ink to suppress the contact line receding and coffee ring effect during inkjet printing. *Colloids Surf. A Physicochem. Eng. Asp.* **2020**, *602*, 125111. [[CrossRef](#)]
39. Hoath, S.D.; Harlen, O.G.; Hutchings, I.M. Jetting behavior of polymer solutions in drop-on-demand inkjet printing. *J. Rheol.* **2012**, *56*, 1109–1127. [[CrossRef](#)]
40. Du, Z.; Yu, X.; Han, Y. Inkjet printing of viscoelastic polymer inks. *Chin. Chem. Lett.* **2018**, *29*, 399–404. [[CrossRef](#)]
41. Du, Z.; Lin, Y.; Xing, R.; Cao, X.; Yu, X.; Han, Y. Controlling the polymer ink's rheological properties and viscoelasticity to suppress satellite droplets. *Polymer* **2018**, *138*, 75–82. [[CrossRef](#)]
42. Jiang, C.; Zhong, Z.; Liu, B.; He, Z.; Zou, J.; Wang, L.; Wang, J.; Peng, J.; Cao, Y. Coffee-Ring-Free Quantum Dot Thin Film Using Inkjet Printing from a Mixed-Solvent System on Modified ZnO Transport Layer for Light-Emitting Devices. *ACS Appl. Mater. Interfaces* **2016**, *8*, 26162–26168. [[CrossRef](#)]

Disclaimer/Publisher's Note: The statements, opinions and data contained in all publications are solely those of the individual author(s) and contributor(s) and not of MDPI and/or the editor(s). MDPI and/or the editor(s) disclaim responsibility for any injury to people or property resulting from any ideas, methods, instructions or products referred to in the content.